Nuclear inclusion bodies of mutant and wild-type p53 in cancer

Journal of Pathology
J Pathol 2017; **242:** 24–38
Published online 23 March 2017 in Wiley Online Library (wileyonlinelibrary.com) DOI: 10.1002/path.4872

ORIGINAL PAPER

Nuclear inclusion bodies of mutant and wild-type p53 in cancer: a hallmark of p53 inactivation and proteostasis remodelling by p53 aggregation

Frederik De Smet[1,2,3,4†], Mirian Saiz Rubio[1,2†], Daphne Hompes[5], Evelyne Naus[1,2], Greet De Baets[1,2], Tobias Langenberg[1,2], Mark S Hipp[6], Bert Houben[1,2], Filip Claes[1,2], Sarah Charbonneau[3], Javier Delgado Blanco[1,2], Stephane Plaisance[7], Shakti Ramkissoon[3,8,9], Lori Ramkissoon[3], Colinda Simons[10], Piet van den Brandt[10], Matty Weijenberg[10], Manon Van England[11], Sandrina Lambrechts[12], Frederic Amant[12,13], André D'Hoore[5], Keith L Ligon[3,4,8,9,14], Xavier Sagaert[15], Joost Schymkowitz[1,2*] and Frederic Rousseau[1,2*]

[1] *The Switch Laboratory, Department of Cellular and Molecular Medicine, KU Leuven, Leuven, Belgium*
[2] *VIB Center for Brain and Disease Research, Leuven, Belgium*
[3] *Department of Medical Oncology, Center for Molecular Oncologic Pathology, Dana-Farber Cancer Institute, Boston, MA, USA*
[4] *The Broad Institute, Cambridge, MA, USA*
[5] *Department of Abdominal Surgery, University Hospitals Gasthuisberg, Leuven, Belgium*
[6] *Department of Cellular Biochemistry, Max Planck Institute of Biochemistry, Martinsried, Germany*
[7] *Nucleomics Core, Flanders Institute for Biotechnology (VIB), Leuven, Belgium*
[8] *Department of Pathology, Division of Neuropathology, Brigham and Women's Hospital and Children's Hospital Boston, Boston, MA, USA*
[9] *Department of Pathology, Harvard Medical School, Boston, MA, USA*
[10] *Department of Epidemiology – GROW School for Oncology and Developmental Biology, Maastricht University, Maastricht, The Netherlands*
[11] *Department of Pathology – GROW School for Oncology and Developmental Biology, Maastricht University, Maastricht, The Netherlands*
[12] *Department of Obstetrics and Gynaecology, Division of Gynaecological Oncology, University Hospitals Leuven, KU Leuven, Leuven, Belgium*
[13] *Centre for Gynaecological Oncology Amsterdam, Netherlands Cancer Institute, Amsterdam, The Netherlands*
[14] *Department of Pathology, Children's Hospital Boston, Boston, MA, USA*
[15] *Translational Cell and Tissue Research, KU Leuven, Leuven, Belgium*

**Correspondence to: F Rousseau or J Schymkowitz, The Switch Laboratory, Department of Cellular and Molecular Medicine, KU Leuven, and the VIB Centre for Brain and Disease Research, Leuven, B-3000, Belgium. E-mail: Frederic.rousseau@switch.vib-kuleuven.be; Joost.Schymkowitz@switch.vib-kuleuven.be*

†Equal contributions.

Abstract

Although p53 protein aggregates have been observed in cancer cell lines and tumour tissue, their impact in cancer remains largely unknown. Here, we extensively screened for p53 aggregation phenotypes in tumour biopsies, and identified nuclear inclusion bodies (nIBs) of transcriptionally inactive mutant or wild-type p53 as the most frequent aggregation-like phenotype across six different cancer types. p53-positive nIBs co-stained with nuclear aggregation markers, and shared molecular hallmarks of nIBs commonly found in neurodegenerative disorders. In cell culture, tumour-associated stress was a strong inducer of p53 aggregation and nIB formation. This was most prominent for mutant p53, but could also be observed in wild-type p53 cell lines, for which nIB formation correlated with the loss of p53's transcriptional activity. Importantly, protein aggregation also fuelled the dysregulation of the proteostasis network in the tumour cell by inducing a hyperactivated, oncogenic heat-shock response, to which tumours are commonly addicted, and by overloading the proteasomal degradation system, an observation that was most pronounced for structurally destabilized mutant p53. Patients showing tumours with p53-positive nIBs suffered from a poor clinical outcome, similar to those with loss of p53 expression, and tumour biopsies showed a differential proteostatic expression profile associated with p53-positive nIBs. p53-positive nIBs therefore highlight a malignant state of the tumour that results from the interplay between (1) the functional inactivation of p53 through mutation and/or aggregation, and (2) microenvironmental stress, a combination that catalyses proteostatic dysregulation. This study highlights several unexpected clinical, biological and therapeutically unexplored parallels between cancer and neurodegeneration.

Keywords: p53 aggregation; proteostasis; colon cancer; glioblastoma; nuclear inclusion bodies

Received 17 June 2016; Revised 20 December 2016; Accepted 27 December 2016

No conflicts of interest were declared.

Introduction

The cellular protein quality control (PQC) machinery of chaperones and proteases ensures protein homeostasis or 'proteostasis' [1–3]. Because of ageing, mutation, or (patho-)physiological insults [4], the processing of misfolded proteins becomes less efficient, and this can lead to protein accumulation and aggregation, and vice versa [1–3]. Abnormal protein aggregation causes well-known misfolding diseases, including neurodegenerative and amyloidogenic disorders [1–3], in which there is typically accumulation of disease-specific proteins in inclusion bodies or extracellular deposits [1–3]. In rare familial cases, germline mutations increase the aggregation propensity of disease-specific proteins, the chronic expression of which is believed to initiate a vicious cycle of proteostatic dysregulation and aggregation. In the more common sporadic conformational diseases, age-associated erosion of PQC is more likely to cause wild-type protein aggregation.

The tumour suppressor p53 is the most commonly mutated gene in cancer [5]. Most mutations occur in the DNA-binding domain and can be categorized according to their conformational effect: whereas 'contact' mutations alter DNA-binding properties without disturbing the overall folding, 'structural' mutations disrupt the native fold [6,7]. Inactivity of p53 commonly correlates with its aberrant accumulation in cancer cells [5,8], which was initially explained by an impeded human double minute-2 (MDM2) response that mediates p53 degradation [9]. Recently, we and others showed that aggregation can also contribute to p53 inactivation, accumulation and gain-of-function activities [10–18]. Importantly, although mutation often increases the aggregation propensity of p53 by destabilizing its structure, wild-type p53 (p53-WT) is itself already thermodynamically labile (T_{melt} of 42 °C) [10,15,16]. As ageing favours both mutation and proteostatic decline, the aggregation of both mutant p53 and p53-WT might be a common and possibly physiology-modifying event. The accumulation of p53 aggregates has been previously reported by us and others in tumour lines transiently overexpressing mutant p53 or in sparse human tumours [13,14,17,19].

Here, we present a study agglomerating 370 tumour biopsies investigating the presence of p53 aggregates in cancer. We found that a large fraction of mutant and p53-WT-positive tumours contain nuclear inclusion bodies (nIBs) of inactive p53 that co-localize with known markers for aggregates in neurodegeneration. The presence of aggregated p53 in cell lines and nIBs in tumours was associated with a distinctive proteostatic profile and patient survival.

Materials and methods

Cell lines

Cells were grown in standard conditions [Dulbecco's modified Eagle's medium (DMEM)/10% fetal bovine serum (FBS); Life Technologies, Gent, Belgium]. Stress insults included hypoxia (0.5% oxygen), proteostatic stress (0.5 μM MG132, M7449; Sigma-Aldrich, Overijse, Belgium), hypoglycaemia (DMEM without glucose), and oxidative stress (100 μM $NiCl_2$).

Sodium dodecyl sulphate (SDS)-gradient blue native polyacrylamide gel electrophoresis (BN-PAGE) analysis

Cells were lysed in 150 mM NaCl, 50 mM Tris–HCl (pH 8), 1% IGEPAL(NP40), 1 × Complete inhibitor (Roche, Vilvoorde, Belgium), and 1 U/μl Universal Nuclease (Pierce, Leuven, Belgium), and this was followed by incubation with SDS as indicated. BN-PAGE analysis was performed as described previously [17].

Clinical samples

Stage II/III colon cancer samples ($n = 163$) were collected by the Department of Abdominal Surgery (2004–2006; UZLeuven, Belgium; project #S53472), and glioblastoma (GBM) samples ($n = 58$, only isocitrate dehydrogenase $1/2^{WT}$) were collected by the Center for Molecular Oncologic Pathology [2007–2013; Dana-Farber Cancer Institute, Boston, MA, USA; Institutional Review Board protocol 10–417]. Patients were monitored for tumour recurrence and overall survival (median follow-up: 50.2 months for colon cancer and 17 months for GBM).

Antibodies

The antibodies used were as follows: anti-p53 DO-1 and FL393, anti-HSC70, anti-HSP90, anti-HSPA6, anti-DNAJB1, and anti-sigma-1 receptor (SigmaR) (Santa Cruz Biotechnology, Heidelberg, Germany); anti-promyelocytic leukaemia (PML), anti-nucleolin, anti-SQSTM1, anti-HDAC6, anti-BAG2, and anti-heat shock transcription factor 1 (HSF1) (Abcam, Cambridge, UK); anti-HSP70 (Cell Signaling Technology, Leiden, The Netherlands); and A11(AHB0052), Alexa-labelled secondary antibodies, and 4′,6-diamidino-2-phenylindole (DAPI) (Life Technologies). Proximity ligation was performed with Duolink (Olink, Uppsala, Sweden) according to the manufacturer's instructions.

Statistical analysis

Statistical analyses were performed in R-studio (v0.97.551) with R (v3.0.1) or GraphPad Prism 6.0. Kaplan–Meier estimates were used to create survival curves. The Cox proportional hazard model and the score log rank test were used to determine statistical significance. Pairwise comparisons were performed by the use of likelihood ratio tests with Bonferroni corrections. Non-parametric Kruskal–Wallis statistics with Bonferroni correction were used for pairwise comparisons of high-content data.

Additional methods

See supplementary materials and methods for additional methods.

Results

nIBs of p53

Aggregation-related diseases are typically characterized by the abnormal accumulation and aggregation of disease-specific proteins [1,3], often observed as intracellular inclusions and/or extracellular deposits [2]. To search for p53 aggregation phenotypes, we used immunofluorescence staining with sufficient sensitivity to quantify overall expression levels and also to detect subcellular inhomogeneities (e.g. inclusion bodies) and aberrant subcellular localization.

Staining of a cohort of colon cancer samples ($n = 163$) revealed various subcellular p53 phenotypes: 71% of the p53-positive tumours contained p53-positive 'puncta' within the diffuse p53 staining pattern of the nucleus in a subset of tumour cells [p53-positive nIBs (p53-nIBs)], whereas the remainder showed homogeneous, diffuse nuclear p53 staining throughout the tumour (Table 1; Figure 1A, B; supplementary material, Figure S1A–H). The occurrence of p53-nIBs was often associated with cytosolic staining of lower intensity at a similar frequency (Table 1). Occasionally, we observed cytoplasmic p53 staining without the presence of nIBs, and pure cytoplasmic IBs were only observed once (Figure 1C, D). According to these observations, we defined five subcategories: tissue without p53 expression (NULL); tissue with diffuse, well-dispersed nuclear p53 (SOLUB); tissue with p53-nIBs in >50% of tumour cells (NUCINC50); tissue with p53-nIBs in 1–5% (NUCINC5) of tumour cells; and tissue with diffuse p53 in the nucleus and cytoplasm (CYTO). Markedly, this classification could not be made reliably by the use of 3,3′-diaminobenzidine /horseradish peroxidase staining (supplementary material, Figure S1I–L), explaining why this had not been described earlier.

Also in biopsies from GBM, colon cancer, ovarian cancer, endometrial cancer, melanoma, and Barrett's oesophagus, we observed p53-nIBs at a tumour type-specific frequency in samples originating from all contributing institutes with both monoclonal and polyclonal antibodies (Table 1; Figure 1E; supplementary material, Figure S1). p53-nIBs therefore constitute a genuine and widespread, but so-far uncharacterized, phenotype. Also in lymph nodes containing metastatic colon cancer cells, the p53 phenotype of the primary tumour was generally maintained (supplementary material, Table S1).

Biopsies containing p53-nIBs were subsequently co-stained with amyloid dyes [i.e. luminescent conjugated oligothiophenes (LCOs)] [20] or the conformational-specific antibody A11, which recognizes oligomeric aggregates [21]. Although we did not observe specific LCO staining (suggesting that p53 did not generate textbook amyloids *in vivo*), p53/p53-nIBs and A11 did co-localize in ovarian tumours using proximity ligation (supplementary material, Figure S2), confirming previous findings [14] and showing that p53 was primarily present as oligomeric aggregates. However, the A11 staining was insufficiently reliable and robust for routine screening, forcing us to use p53-nIB detection as a readout.

nIBs contain transcriptionally inactive mutant p53 or p53-WT

Following p53 genotyping, we observed that, although favoured by p53 mutation, homogeneous and nIB phenotypes were present in both p53-WT and mutant tumours (Figure 1F, G; supplementary material, Table S3). In the p53-positive samples, p53 transcriptional activity (as measured by *MDM2* mRNA levels) was also significantly higher in samples containing SOLUB-WT than in those containing NUCINC50-WT (Figure 1H), whereas no difference was found between the NUCINC50-WT group and the p53-NULL group, showing severe impairment of p53 activity when it is present in nIBs. Expression levels of p21 and BAX were highly variable (supplementary material, Figure S2D, E), suggesting p53-independent mechanisms [22–24]. *TP53* mRNA levels were lower in the NULL samples than in the p53-positive samples (Figure 1I), suggesting genetic aberrations.

Mutant p53 accumulates in the nucleus as soluble oligomeric aggregates

Next, we phenotyped 22 tumour cell lines that endogenously express wild-type, contact or structurally destabilized mutant p53 (Table 2). When we analysed thousands of single cells under baseline conditions by using immunofluorescence high-content imaging, p53 was primarily observed in a diffuse pattern in the nucleus, as is commonly observed [25], and only $5.1 \pm 3.1\%$ of cells showed a small number of nIBs (<2 nIBs per cell). We also determined p53's folding status by immunoprecipitation (IP) with p53-specific conformational antibodies (i.e. pAb1620 for native p53 and pAb240 for misfolded p53) [26]: whereas p53-WT and contact mutants largely adopted the native/pAb1620-positive conformation, structural mutants predominantly adopted the misfolded/pAb240-positive conformation (Table 2; supplementary material, Figure S3A).

Given the overall absence of nIBs in standard cell culture conditions (in contrast to biopsies) and the A11 positivity of p53 in biopsies, p53 was expected to form small oligomeric aggregates, similarly to what is seen in neurodegenerative diseases, where the presence of soluble oligomeric aggregate precursors is often indicative of pathological activity [1,27]. Previously, we optimized a BN-PAGE method that discriminates between native tetrameric p53 and aggregated/oligomeric forms, which are recognized by a continuous high molecular weight

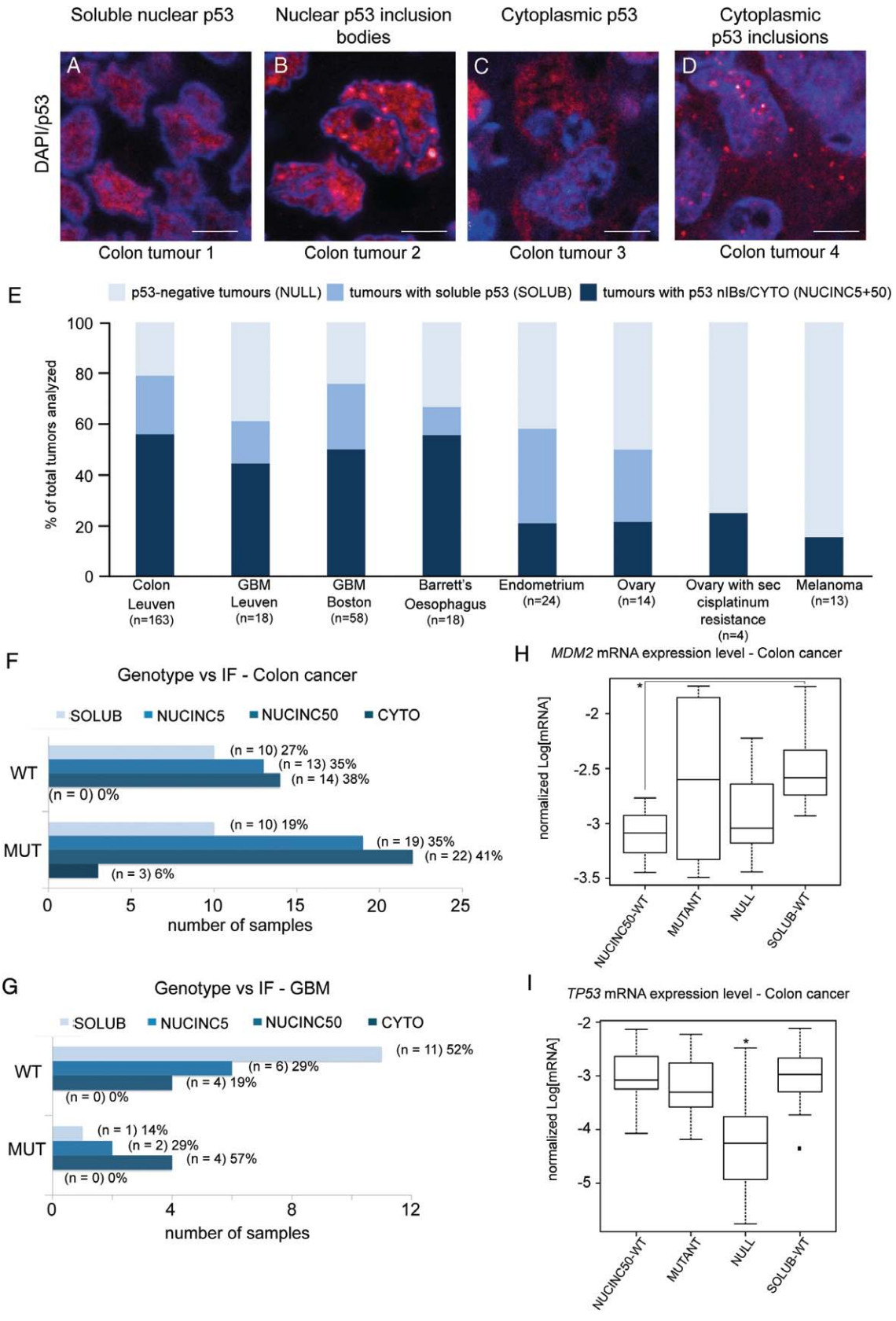

Figure 1. Staining of cancer biopsies reveals the presence p53-nIBs. (A–D) p53 immunofluorescence staining of colon cancer biopsies. (A–D) Overlay of confocal images stained for p53 (red) and with nuclear DAPI staining (blue). (E) Quantification of the number of tumours that are p53-positive and/or contain p53 inclusions in various tumour types, as indicated. (F, G) Bar chart distribution of the inclusion body phenotype in p53-WT or mutant (MUT) populations of colon cancer (F) and GBM (G). (H, I) For the transcriptional analysis, patient samples were divided into four subgroups: NUCINC50-WT (p53-WT nIBs with >50% of tumour cells containing p53-nIBs), MUT (mutant p53 with nIB or diffuse p53 staining), NULL (without p53 expression), and SOLUB-WT (diffuse, p53-WT), in which *MDM2* (H) or p53 (I) mRNA levels were measured with the n-string method in extracted RNA from 86 colon tumour biopsies. *Statistically significant.

smear [17]. This procedure was further adapted to titrate the stability of the aggregates by applying increasing concentrations of SDS, a protein-denaturing detergent. Here, p53-WT showed little resistance to SDS, and consisted mainly of native tetrameric p53, which readily disassembled into monomers (Figure 2A; supplementary material, Figure S3B). In all mutant tumour lines, we observed high molecular weight smears. Whereas, for the contact mutant, this smear was entirely resolved above 0.2% SDS, this smear persisted until 0.6% SDS for structural/pAb240-positive mutants (Figure 2A; supplementary material, Figure S3C). Moreover, the gradual disappearance of this high molecular weight smear correlated with the appearance of SDS-stable octamers and tetramers along with monomeric p53 (supplementary material, Figure S3D). In comparison, p53-WT tetramers already disassembled into monomers below 0.2% SDS (Figure 2A; supplementary material, Figure S3B–D), suggesting that tetramers emerging from these high molecular weight smears are distinct from native p53 tetramers and are stabilized by non-native interactions.

Aggregated proteins are usually also more resistant to proteolytic cleavage while misfolded proteins are generally more sensitive [28,29]. A dose–response study with proteinase K (ProtK) was therefore applied to cell extracts (Figure 2B), and showed that p53-WT was more resistant to proteolytic degradation at low ProtK concentrations (owing to its folded structure), whereas mutant p53 was readily cleaved, demonstrating its misfolded nature. However, proteolytic fragments of mutant p53 were also more resistant to higher ProtK concentrations and persisted at concentrations at which p53-WT was already completely digested, confirming not only the misfolded but also aggregated nature of p53.

Finally, whereas the majority of p53 was present in the soluble fraction, we also identified a small (<5%) insoluble p53 fraction by using an SDS-based extraction protocol, adopted from procedures to for extracting amyloid-β plaques from Alzheimer brain tissue [30,31]. This showed that cell lines containing pAb240-positive mutants consistently had more insoluble p53 that resisted higher SDS concentrations (up to 0.6%) than p53-WT or contact mutants (<0.1%; Figure 2C). This demonstrates that misfolded p53 not only forms more stable soluble aggregates, but also forms more stable insoluble aggregates. Proteolytic cleavage analysis also showed that insoluble p53 aggregates were more resistant to ProtK than the soluble aggregates, even though they shared similar digestion patterns (Figure 2B). This confirms the aggregated nature of insoluble p53, and suggests that this results from the maturation and stabilization of soluble aggregates. Even though amyloid-like p53 structures had been found before in only a few tumours, by the use of thioflavin T binding, Congo Red birefringence, and amyloid-specific antibodies [10,18,32], the current study on a larger panel of tumour cell lines and biopsies suggests that nuclear p53 aggregates do not generally mature into ordered amyloid fibrils [17].

Aggregated p53 assembles into nIBs as a result of tumour-associated stress

The appearance of p53 aggregates in patient biopsies as nIBs versus oligomeric aggregates in cell lines is highly reminiscent of findings made in pathologies with a more established connection to protein aggregation. Several reports have described diffuse staining patterns of huntingtin, the protein causing Huntington's disease, under ideal cell culture conditions, and have demonstrated that

Table 1. Quantification of the different aggregation phenotypes observed by immunofluorescence in colon cancer and glioblastoma

		Colon cancer		Glioblastoma	
	Category	*n*	%	*n*	%
Nuclear staining	No p53 staining	34	20.9	15	25
	Nuclear p53 staining	129	79.1	45	75
	Total	163		60	
Nuclear inclusions	No p53 staining	34	20.9	15	25
	p53 staining, no nuclear inclusions	38	23.3	17	28.3
	p53 staining, <5% nuclear inclusions	48	29.4	15	25
	p53 staining, >50% nuclear inclusions	43	26.4	13	21.7
	Total	163		60	
Cytoplasmic staining	No p53 staining	34	20.9	15	25
	p53 staining, no cytoplasmic stain	92	56.4	39	65
	p53 staining, <5% cytoplasmic stain	29	17.8	5	8.3
	p53 staining, >50% cytoplasmic stain	8	4.9	1	1.7
	Total	163		60	
Cytoplasmic inclusions	No p53 staining	34	20.9	15	25
	p53 staining, no cytoplasmic inclusions	125	76.7	43	71.6
	p53 staining, <5% cytoplasmic inclusions	3	1.8	2	3.3
	Nuclear p53 staining, >50% cytoplasmic inclusions	1	0.6	0	0
	Total	163		60	
Cytoplasmic staining and nuclear inclusions	No	133	81.6	58	96.7
	Yes	30	18.4	2	3.3
	Total	163		60	

Table 2. Overview of the genetic and biochemical parameters of endogenous p53 in various tumour cell lines

Cell line	Tumour type	p53 genotype	Pseudo-ΔΔ*G* (FoldX)	Total p53 expression (MSD)	BN-PAGE	0.5% SDS resistance?	IP pAB1620	IP pAB240
Saos2	Osteosarcoma	Null	Null	0	Not detectable	ND	ND	ND
A549	Lung	WT	0	1623	Not aggregating	No	2	0
HEK293	Human embryonic kidney	WT	0	11 507	Not aggregating	No	2	1
LnCAP	Prostate	WT	0	587	Not detectable	ND	0	0
HCT116	Colon	WT	0	6398	Not aggregating	No	2	0
U2OS	Osteosarcoma	WT	0	863	Not aggregating	No	1	0
SBC5	Lung	R248L	0.03	16 504	Not aggregating	No	2	0
SW1783	Astrocytoma	R273H	1.03	105 286	Not aggregating	No	2	1
U251	Gliobastoma	R273H	1.03	70 207	Not aggregating	No	2	1
Widr	Colon	R273H	1.03	159 257	Not aggregating	No	2	2
PLCPRF5	Liver	R249S	1.03	4678	Not aggregating	No	1	2
HT1376	Bladder	P250L	1.57	25 372	Aggregating	Partial	2	2
C33A	Retinoblastoma	R273C	1.65	35 906	Mildly aggregating	No	2	2
SKNSH	Neuroblastoma	R156P	3.53	79 583	Aggregating	Yes	0	2
CHL1	Melanoma	H193R	3.63	18 972	Aggregating	Yes	1	2
Mel1617	Melanoma (skin)	Y220C	4.15	8547	Aggregating	Yes	0	2
HCC827	Lung	V218	>5	19 608	Aggregating	Yes	0	2
Ln405	Glioblastoma	R282W	>5	22 826	Aggregating	No	0	2
HACAT	Immortalized skin	R282W/H179Y	>5	121 295	Mildly aggregating	Partial	2	2
Du145	Prostate	P223L/V274F	>5	25 054	Aggregating	Yes	0	2
Detroit562	Pharynx	R175H	>5	79 770	Aggregating	Yes	0	2
VMCUB	Bladder	StopY126/R175H	>5	301	Not detectable	ND	ND	ND

BN-PAGE, blue native polyacrylamide gel electrophoresis; IP, immunoprecipitation; Mesoscale Discovery ELISA (MSD); ND, not determined; WT, wild-type; 0, no signal; 1, low signal; 2, high signal.
The pseudo-ΔΔG (kcal/mol) is a measure of the destabilizing effect of the mutation as measured by the FoldX force field (the higher the value, the more destabilizing the mutation).

a simple proteostatic insult, e.g. exposure to proteasomal inhibitors (e.g. MG132), results in the immediate formation of inclusion bodies, similar to observations made in patients [33,34]. Here, exposure to MG132 also resulted in the formation of p53-nIBs in a set of pAb240-positive lines (Figure 3A). In addition, $29 \pm 6\%$ of cells from the pAb240-positive cell lines had >5 inclusions per cell upon MG132 exposure, as opposed to $5.1 \pm 3.1\%$ that showed only >2 inclusions per cell under baseline conditions, whereas cell lines containing p53-WT showed only minimal induction of nIBs upon MG132 exposure.

Exposure to additional tumour-related, microenvironmental stress, including hypoxia, hypoglycaemia, oxidative stress, and/or proteostatic stress, confirmed that cell lines containing mutant p53 were readily inclined to form nIBs (Figure 3B). Interestingly, exposure to a combination of stress conditions also resulted in the formation of p53-nIBs and aggregates in p53-WT cell lines (Figure 3C–E; supplementary material, Figure S4A) [17]. Finally, whereas MG132 treatment resulted in minimal changes in the overall p53 levels, we observed a shift from the soluble to the insoluble fraction (Figure 3F), comparable to aggregating proteins in neurodegeneration [35]. The insoluble p53 fraction was also more SDS-resistant for aggregating p53 mutants, even though we also observed a small, but detectable insoluble fraction in p53-WT and contact mutants (Figure 3F).

To analyse the correlation of p53's transcriptional activity with its presence in nIBs, we used HCT116^{p53WT} cells, in which p53 becomes transcriptionally activated upon exposure to cisplatin. In baseline conditions, exposure to cisplatin resulted in a significant induction of p53-responsive genes (*p21*, *MDM2*, and *PUMA*), strikingly without the formation of p53-nIBs (Figure 3G). However, after exposure to a combination of cisplatin and cellular stress (i.e. MG132 and/or hypoxia), the p53 response was dampened proportionally to the number of p53-nIBs (Figure 3G), suggesting that the observed nIBs are primarily proteostatic sinks of non-functional protein.

Overall, cellular stress can inactivate p53 through aggregation and induce the formation of p53-nIBs, a phenotype that is readily achieved for structurally destabilized mutants, but can also be observed for p53-WT or contact mutants. The impact of proteostatic stress on nIB formation in cell lines might also explain the observed offset between aggregation and inclusion body formation in this and an earlier study [17].

p53-nIBs are PML-positive and SigmaR-positive

Various known nIB markers were analysed, of which the nuclear body markers PML (Figure 4A–E) and SigmaR (Figure 4F) co-localized with p53-nIBs, whereas the nucleolar marker nucleolin primarily did not (supplementary material, Figure S4B) [36]. SigmaR was recently identified as a marker for neurodegenerative nIBs [37], suggesting the presence of molecular parallels between cancer and neurodegeneration. PML has been detected in nIBs containing polyglutamine proteins in patients with neurodegeneration, but has also been connected to p53. Because PML-positive nIBs have been linked to both the activation of p53-WT and to gain of function by mutant p53 [38,39], we further analysed p53's transcriptional functionality under

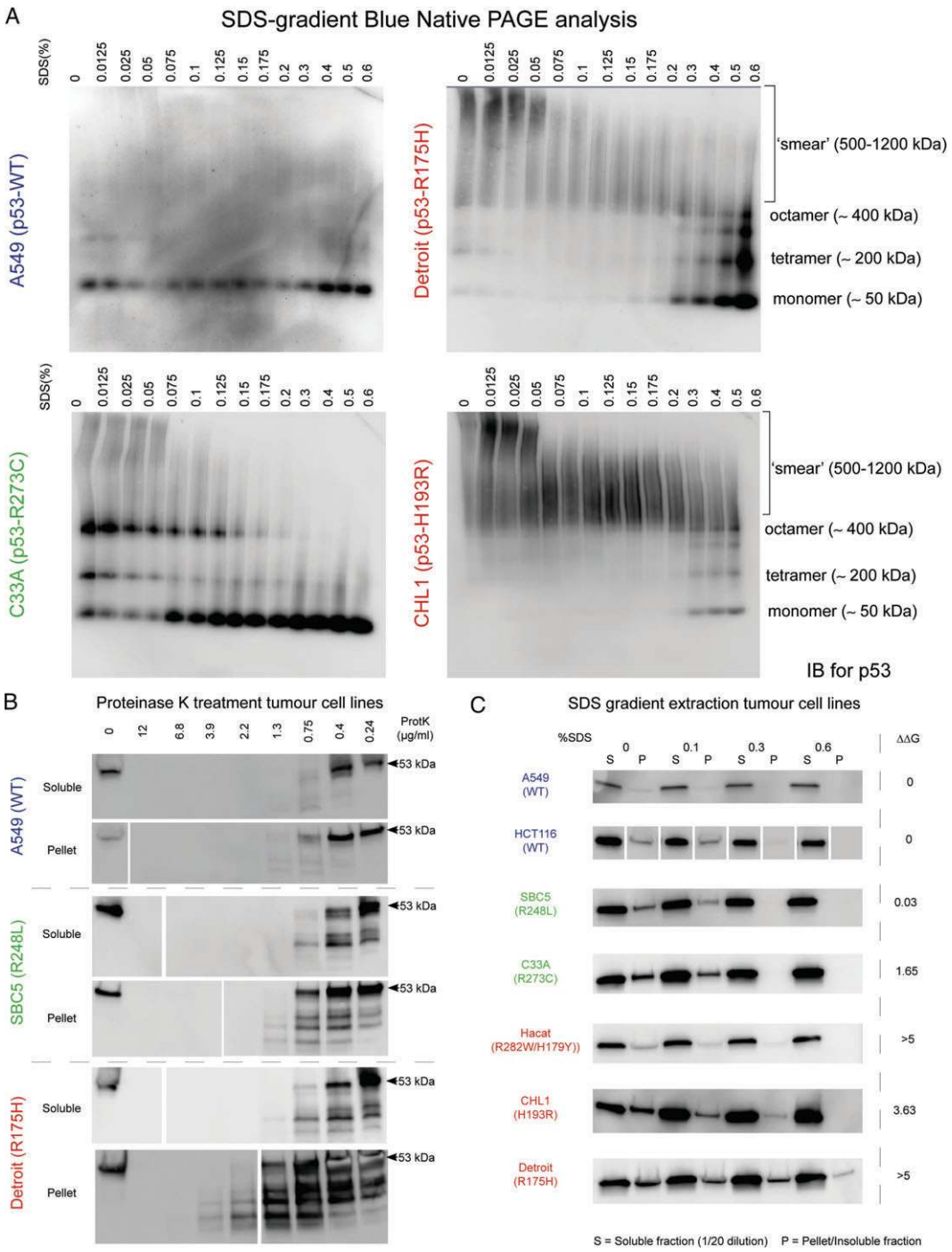

Figure 2. Biochemical analysis of endogenous p53 in various tumour cell lines (A) Representative examples of immunoblots for p53 (DO-1 antibody) following SDS-gradient BN-PAGE analysis at the indicated SDS concentrations (%) for four different tumour cell lines. (B) Immunoblots for p53 (DO-1 antibody) following ProtK treatment at the indicated concentrations (µg/ml) for 15 min at 37 °C of the soluble and the pellet fractions from various tumour cell lines endogenously expressing p53. (C) Immunoblots for p53 (DO-1 antibody) following SDS-gradient extraction with the indicated SDS concentration (%) from various tumour cell lines endogenously expressing p53. P, pellet fraction; S, soluble fraction (diluted 1/20). The pseudo-$\Delta\Delta G$ values are indicated on the right of the blots.

baseline conditions and upon cisplatin or MG132 treatment (supplementary material, Figure S4C, D). In contrast to the p53-WT cell lines, none of the mutant p53 proteins could induce MDM2. IP with the conformational antibodies (see above) revealed that exposure to MG132 resulted in a loss of well-folded p53, whereas the misfolded conformation was maintained (Figure 4G). Finally, double staining of p53 with PML or SigmaR confirmed that these markers also co-localized with p53-nIBs in biopsies (Figure 4H–S).

Overall, proteostatic stress can lead to transcriptionally dead, misfolded, aggregated p53, which can be assembled in PML/SigmaR-positive nIBs upon microenvironmental stress. In addition to being p53 activation sites [38,40–42], these bodies also seem to function as nuclear aggreosomes, as previously

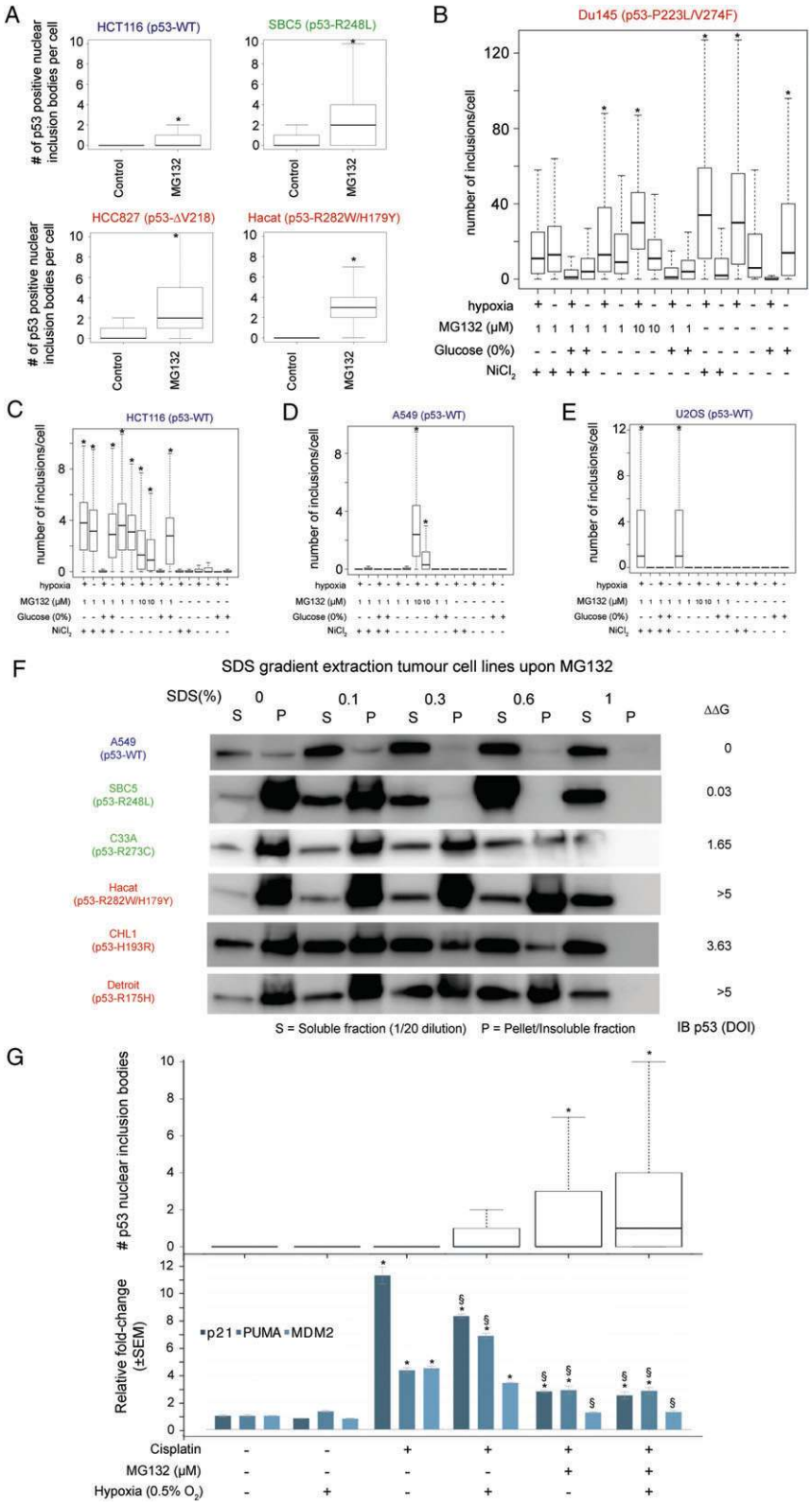

Figure 3. Tumour-associated stress induces the formation of p53-nIBs. (A) Quantification of high-content screening showing boxplot analysis of the number of p53-nIBs per cell in control conditions and upon MG132 treatment (10 μM) in the indicated tumour cell lines. (B–E) Quantification of high-content screening showing boxplot analysis of the number of p53-nIBs per cell in control conditions, and upon the application of various tumour-associated stress conditions, including 0.2% hypoxia, proteotoxic stress induced by 1 or 10 μM MG132, hypoglycaemia (0% glucose in DMEM/10% FBS), or oxidative stress caused by treatment with $NiCl_2$ (100 μM). (F) Immunoblots (IB) for p53 (DO-1 antibody) following SDS-gradient extraction with the indicated SDS concentrations (%) from various tumour cell lines endogenously expressing p53 upon MG132 treatment (10 μM for 8 h). P, pellet fraction; S, soluble fraction (diluted 1/20). The pseudo-$\Delta\Delta G$ values are indicated on the right of the blots. (G) Parallel analysis of the HCT116 cell line upon exposure to various conditions (indicated below the panels) of (top) high-content images for the presence of p53-nIBs and (bottom) mRNA expression of p53 target genes. *Statistically significant as compared with the control condition. §Statistically significant as compared with the cisplatin treatment condition.

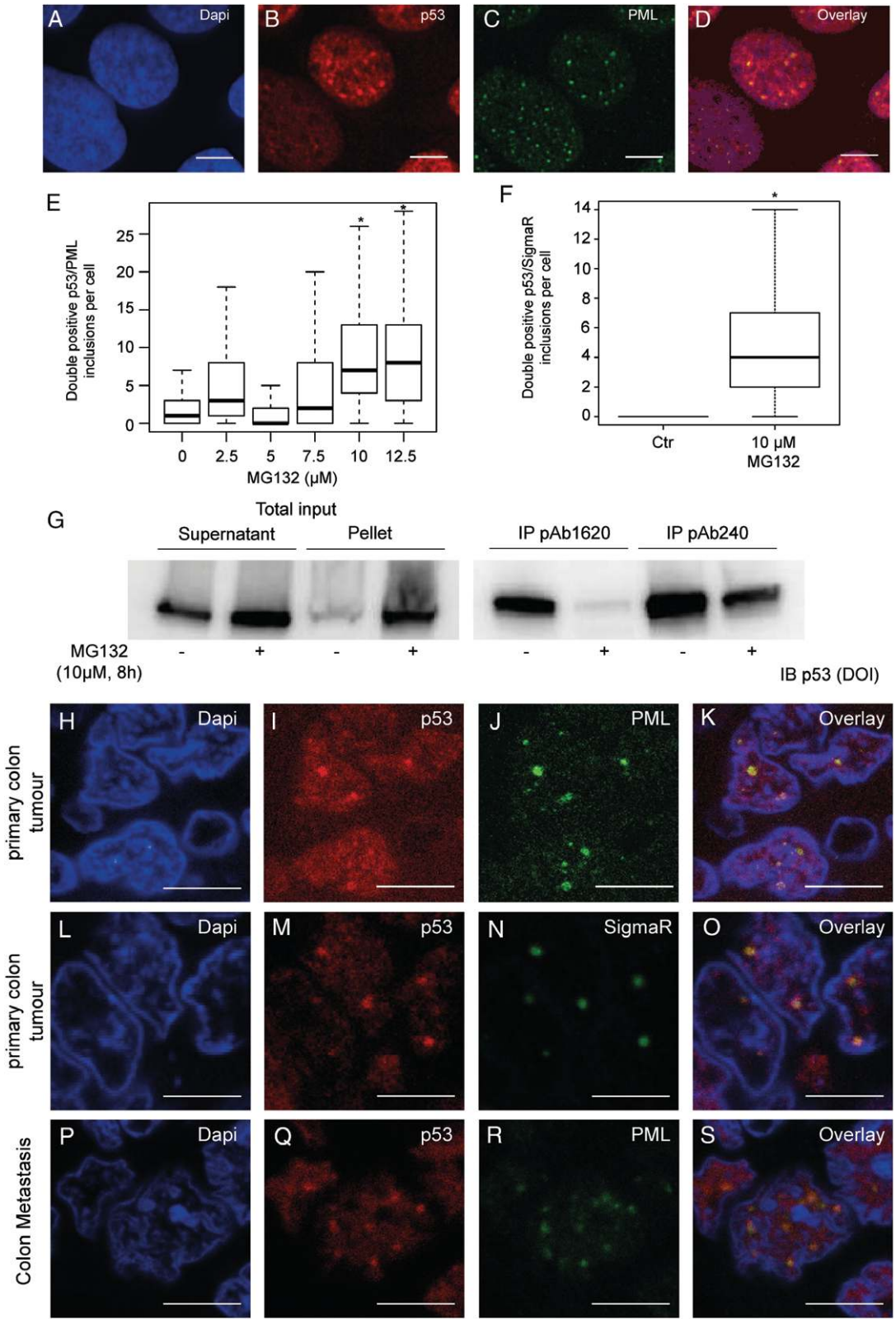

Figure 4. p53-nIBs are PML-positive and SigmaR-positive, and contain misfolded p53. (A–F) Immunofluorescence staining of the HACAT tumour cell line showing nuclei (A, DAPI, blue), p53 staining with the DO-1 antibody (B, red), PML staining (C, green) and the overlay (D) and the quantification upon high-content screening, showing boxplot analysis of the number of p53/PML-double-positive nIBs per cell (E) and the percentage over the total number of p53-nIBs (F). Scale bars: 10 μm in all panels. (G) Immunoblots (IB) for p53 with DO-1 of HACAT cell lysates of control and MG132-treated cells as indicated. Left panel: total amount of p53 in the supernatant or pellet fraction upon lysis in the presence or absence of MG132. Right panel: immunoprecipitation of the supernatant fraction, shown in the left panel, with the indicated conformational p53 antibodies. (H–S) Immunofluorescence staining of colon cancer biopsies of the primary tumour (H–O) and lymph nodes containing metastatic tumour cells (P–S), showing nuclei (H, L, P; DAPI, blue), p53 staining with the DO-1 antibody (I, M, Q; red), PML staining (J, N, R; green), and the overlay (K, O, S). *Statistically significant as compared with the parental cell line. Ctr, control.

described for aggregating green fluorescent protein (GFP) mutants [43].

Aggregated p53 dysregulates cellular proteostasis

Next, the proteostatic consequences of p53 aggregation in tumour cells were investigated by genetically deleting p53 (Figure 5A; supplementary material, Figures S5A and S6). In a mixture of knockout and unmodified cells that could be discriminated by immunostaining for p53, we simultaneously measured the protein levels of important proteostatic markers, including HSF1, several other constitutive and inducible (co-)chaperones (HSP70, HSC70, HSP90, HSPA6, DNAJB1, and BAG2), and autophagy/aggreosome formation factors (SQSTM1 and HDAC6). By analysing the cells in short term, we also determined the dependency/addiction of the cells to aggregated p53, such as Detroit562 cells, which could not survive long-term without p53 (supplementary material, Figure S5B).

Analysis upon removal of aggregated p53 in Detroit562, CHL1, HACAT and HCC827 cells showed a reduction in the HSF1 protein level of ∼20%, whereas this remained largely unaltered in lines containing p53-WT or contact mutant (Figure 5B; supplementary material, Figure S5C–F). A similar reduction was observed for HSP90 (Figure 5C; supplementary material, Figure S5C–F), which was significantly correlated with HSF1, but also with HSC70, DNAJB1, and HSPA6 (Figure 5C, D; supplementary material, Figure S5C–F). The inducible chaperone HSP70 and the co-chaperone BAG2 did not correlate with p53 aggregation status, even though an overall reduction in HSP70 species was observed upon deletion of p53 (Figure 5D, E; supplementary material, Figure S5C–F). Finally, HDAC6 and SQSMT1 seemed to be mutually exclusive, and followed the HSF1 pattern only occasionally in cell lines containing aggregated p53. This argues that p53 aggregates enhance HSF1 expression and a subset of its constitutive/oncogenic downstream targets [44]. Overall, this demonstrates that aggregated p53 contributes to the hyperactivated proteostatic response, using a mode of action that is distinct from that of non-aggregated p53.

It has also been suggested that protein aggregates impair proteasomal degradation by overburdening the cellular proteostasis network [45]. This was demonstrated by the accumulation of unstable fluorescent reporters consisting of GFP fused to destabilizing degrons upon coexpression with aggregation-prone (mutant) proteins but not with wild-type/non-aggregating variants [45,46]. To probe the effect of p53 aggregation on the ubiquitin–proteasome system (UPS), we overexpressed mCherry-fused p53 variants in a HEK293 cell line stably expressing the Ub^{G76V}–GFP protein, which is degraded by the UPS in baseline conditions, but accumulates in cases of excessive proteasomal burden [45,47]. Ub^{G76V}–GFP strongly accumulated when cells expressed the structurally destabilized $p53^{R175H}$–mCherry above a threshold level, indicating concentration-dependent inhibition of proteasomal degradation. This was not observed when cells expressed p53-WT–mCherry, and only at very high expression levels of the contact mutant $p53^{R273H}$–mCherry (Figure 5G). This observation is highly reminiscent of the overexpression of polyglutamine-expanded aggregation-prone proteins [45], further strengthening the parallels between cancer and neurodegeneration.

Tumours containing p53-nIBs show a differential proteostatic expression profile

Also in patients, tumours are known to have an activated chaperone system, partially explained by elevated HSF1 [44,48]. Targeted transcriptional analysis, based on a pan-cancer microarray analysis from which the most important proteostatic components were extracted (supplementary material, Table S4), of colon cancer biopsies identified a combination of proteostatic components, including HSP27, HSP90, HSC70, HSPA5, HSPA9, PSMB7, PSMD10, and p62/SQSTM1, that was sufficient to differentiate between tumours with p53-nIBs (NUCINC50) and without p53-nIBs (SOLUB and NUCINC5) (Figure 6A, B), but not NULL tumours. This corroborates our *in vitro* findings, and suggests that similar mechanisms are also at play in patients. It is also suggestive of the presence of other aggregating proteins with similar effects.

p53-nIBs are associated with decreased disease-free and overall survival

Finally, we correlated p53-nIB status with clinical follow-up in two distinct cohorts (supplementary material, Tables S5 and S6). Using the p53-defined subgroups, we observed that colon cancer patients bearing tumours with p53-nIBs (NUCINC50) or without p53 expression (NULL) showed a significantly worse clinical outcome than patients with tumours containing soluble (SOLUB) or minimally included (NUCINC5) p53 (Figure 6C, D; supplementary material, Table S2). Owing to its small size, the CYTO group was analysed separately, but it showed a similar trend to that of the NUCINC50 group (supplementary material, Figure S7A, B). Similarly, for GBM, a significant correlation of disease-free and overall survival with p53-nIB status was observed (Figure 6E, F). We did not find a correlation between p53 protein levels and nIB formation (matthews correlation coefficient (MCC) = 0.04), corroborating previous findings that p53 expression levels as such constitute an inadequate marker for disease outcome [8]. In addition, survival analysis with p53 genotype data alone did not reveal a correlation with clinical outcome for either colon cancer or GBM, in line with previous studies [8], whereas subgrouping according to p53-nIB status in the same subset did result in patient stratification (Figure 6G, H; supplementary material, Figure S7C, D). This suggests that p53-nIB status integrates the various aspects of p53 inactivation better than p53 genotype as such. Given the high

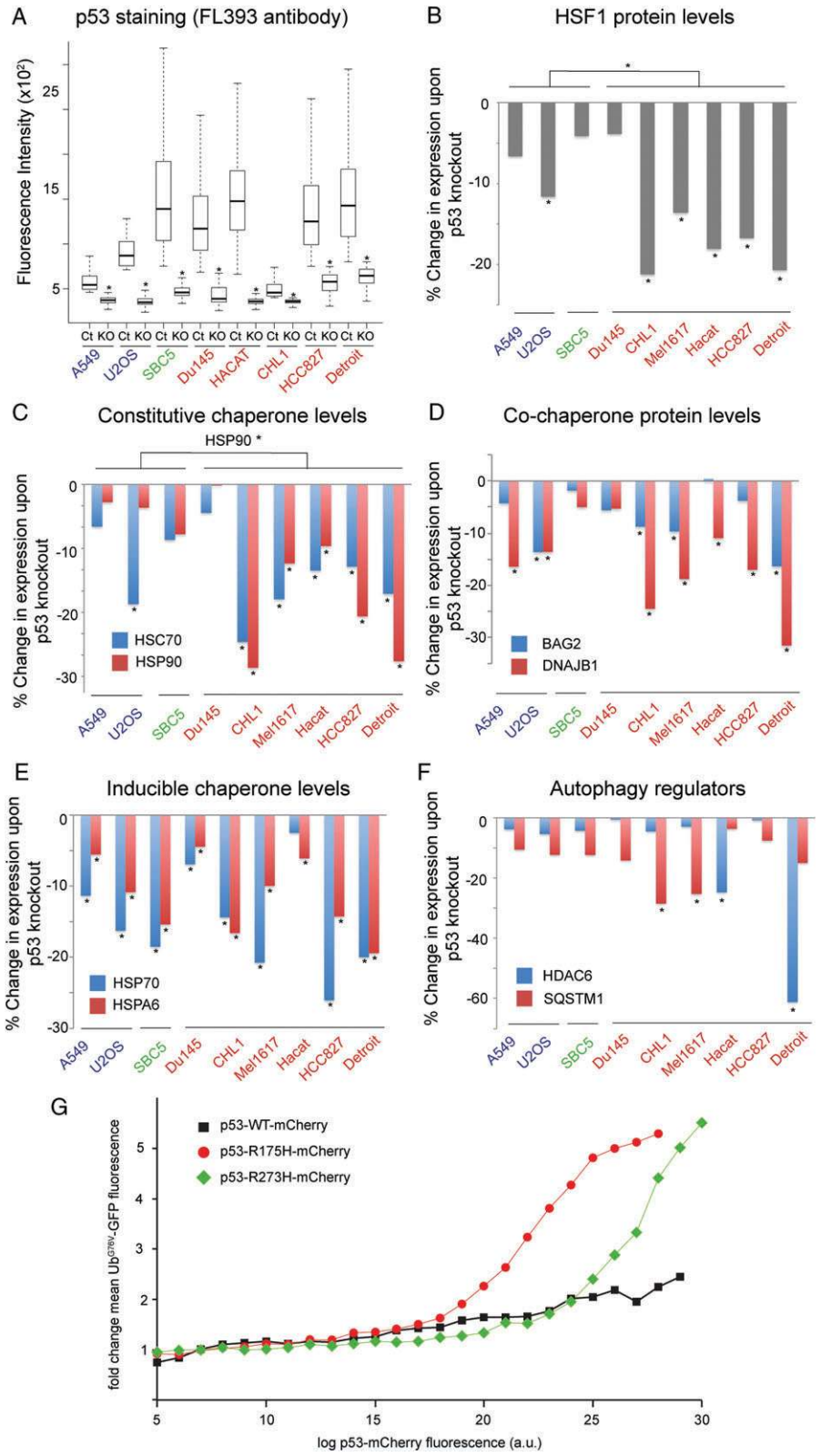

Figure 5. Aggregated p53 alters the proteostatic network of cancer cells. (A) Boxplot representation of the fluorescence intensities measured by high-content imaging in single cells of eight tumour cell lines following p53 immunostaining with the DO-1 antibody (Ct, unmodified control cells; KO, knockout cells). (B–F) Barplots showing the percentage difference between the knockout and parental/control cells of the average intensities of the indicated marker proteins following immunostaining for HSF1 (B), HSC70 and HSP90 (C), BAG2 and DNAJB1 (D), HSP70 and HSPA6 (E), and HDAC6 and SQSTM1 (F). (G) Expression of high levels of mutant p53 leads to stabilization of a reporter for the UPS. HEK293 control and HEK293 cells stably expressing an unstable GFP reporter for the UPS (Ub^{G76V}-GFP) were transfected with p53-WT–mCherry (black squares), p53-R175H–mCherry (red circles) or p53-R273H–mCherry (green diamonds). After 72 h, Ub^{G76V}–GFP levels were analysed by flow cytometry. The relationship between levels of p53 on the *x*-axis and of levels normalized Ub^{G76V}–GFP on the *y*-axis is plotted, and shows concentration-dependent accumulation of Ub^{G76V}–GFP in the presence of mutant p53. The data shown are from a single representative experiment out of three independent repeats. *Statistically significant as compared with the parental cell line.

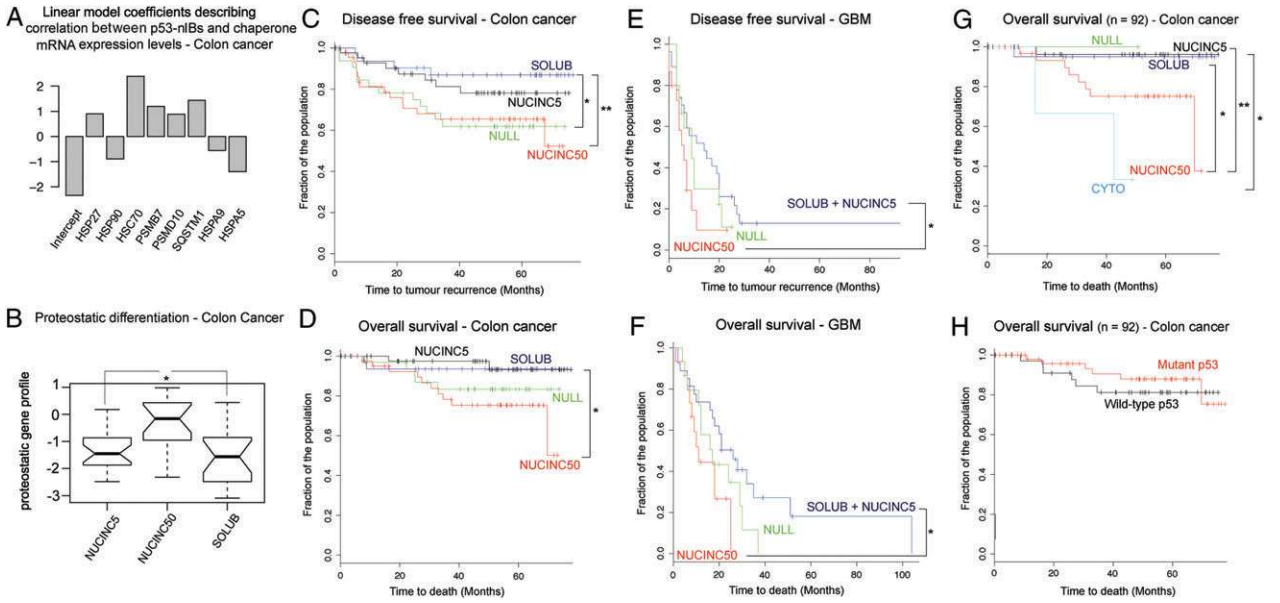

Figure 6. Survival analysis of colon cancer and GBM patients. (A, B) Principle component analysis of the mRNA expression levels for various proteostatic proteins to determine a linear explanatory model. The coefficients for each protein of the model are indicated in (K), and the resulting differentiation between the subcategories is indicated in (L). (C, D) Survival analysis for disease-free survival (DFS) (C) and overall survival (OS) (D) based on the immunofluorescent p53 staining of tissue sections from biopsies of the clinical cohort of colon cancer patients. NUCINC50 versus SOLUB: DFS – hazard ratio = 3.3 (1.1–10.1), $p = 0.024$*; median DFS – 44.4 versus 59.6 months; OS – hazard ratio = 4.6 (1.0–21.2), $p = 0.033$*; median OS – 49.8 versus 62.8 months. Values indicate: mean [95% confidence interval (CI)]. (E, F) Surv ival analysis for DFS (E) and OS (F) based on the immunofluorescent p53 staining of tissue sections from biopsies of GBM patients. NUCINC50 versus SOLUB + AGG1: DFS – hazard ratio = 2.1 (1.03–4.5), $p = 0.040$*; median DFS – 12.5 versus 5 months; OS – hazard ratio = 2.6 (1.2–5.9), $p = 0.020$*; median OS – 21 versus 10 months. (G, H) Survival analysis for OS based on immunofluorescent p53 staining (G) or p53 genotype (H), both of the subset of 92 biopsies of the clinical cohort of colon cancer patients that were subjected to deep sequencing. (G) NUCINC50 versus SOLUB: OS – hazard ratio = 7.0 (0.85–95.3), $p = 0.025$*; median OS – 50.2 versus 61.2 months. (H) p53-WT versus mutant p53: OS – hazard ratio = 0.7 (0.2–2.2), $p = 0.545$; median OS – 49.8 versus 50.6 months. Values indicate: mean (95% CI).

median age of cancer patients, age-related proteostatic dysregulation could have a more profound impact on p53 inactivation than initially expected – echoing the observation that sporadic age-related neurodegenerative diseases frequently involve the aggregation of wild-type proteins as well.

Discussion

We and others have previously shown that p53 can aggregate in cancer [13,14,17], but, as compared with well-known aggregation-associated disorders such as Alzheimer's disease (AD), the clinical relevance of p53 aggregation remains unclear. This study reports the first and largest screen for p53 aggregation phenotypes in 370 biopsies across six different primary and metastatic cancer types by fluorescence immunohistochemistry. We found that the most prevalent p53 aggregation phenotype is the accumulation of p53-positive nIBs of inactive p53-WT or mutant p53, a phenotype reminiscent of neurodegenerative disorders. In hindsight, this finding is not in contradiction with previous studies reporting p53 aggregates in cytoplasmic inclusions [17]: whereas a purely cytoplasmic localization of p53 remains rare, nuclear aggregation of p53 was commonly accompanied by 'cytoplasmic spill-over', suggesting an interplay between the nucleus and the cytoplasm for PQC [49].

Features of p53-nIBs included co-localization with the 'oligomeric aggregate'-specific antibody A11, but also with PML and SigmaR, all of which are markers for (nuclear) protein aggregation in various neurological disorders [49], and also nuclear aggregation of GFP mutants [43]. p53-nIBs primarily did not co-localize to the nucleolus, as opposed to previous observations [50], pointing to lineage-dependent and context-dependent mechanisms [51]. Even though favoured by p53 mutation, the wild-type protein could also be observed in nIBs Functionally, p53-nIBs correlated with a loss-of-function phenotype, as *MDM2* expression was repressed in both p53-WT cell lines and in tumours containing nIBs of p53-WT to the same extent as in p53-null tumours. p53-nIBs therefore constitute a hallmark of p53 protein inactivation through aggregation. Interestingly, nuclear amyloidogenic protein bodies have recently been described as a temporary storage mechanism for proteins in neurons to cope with stress [52]. It remains unknown whether similar mechanisms are at play in cancer.

nIBs containing either p53-WT or mutant p53 are also in accordance with the pathophysiology of established aggregation diseases, in which aggregation can be induced by both mutation (e.g. rare cases of familial AD) and physiological stress associated with ageing [1]. Indeed, the majority of cases of sporadic AD are

associated with wild-type protein aggregation [2]. The apparent genotypic indifference of p53 aggregation in human tumours could therefore be instigated by similar mechanisms. First, as cancer is a disease resulting from the accumulation of genetic lesions, most commonly in p53, the contribution of mutations to protein aggregation should be more common in cancer than in neurodegeneration. This is indeed the case, because, overall, more than half of p53-nIB-positive tumours express mutant p53. Second, during tumour formation and progression, cells are exposed to severe stress conditions such as hypoxia, oxidative and proteostatic stress, and hypoglycaemia [53], which, along with physiological ageing, might explain the aggregation of p53-WT in the remaining nIB-positive tumours.

We investigated this hypothesis by analysing p53 aggregation in cell lines under normal and tumour-associated stress conditions. Under normal growth conditions, structurally destabilized p53 mutants readily formed SDS-resistant and ProtK-resistant aggregates, whereas p53-WT did not aggregate. Tumour-associated stress, on the other hand, enhanced mutant p53 aggregation, but also induced p53-WT aggregation and led to the formation of p53-nIBs of both genotypes in association with the same markers. This confirms the presence of nuclear p53 aggregates, and demonstrates that both mutation and environmental stress can be drivers of the aggregation process. It also recapitulates the distinction between protein aggregation and inclusion body formation of misfolded proteins, another common finding in aggregation-associated diseases. Whereas protein misfolding/aggregation is primarily determined by the intrinsic properties of the protein (i.e. mutants having a higher propensity to aggregate), inclusion body formation is a cellular response to proteostatic stress (and can occur both in the case of stress-induced wild-type aggregation and in the case of mutant aggregation).

Our results also demonstrate that the accumulation of aggregating p53 is not neutral: By removing or overexpressing p53, we showed that aggregated p53 modifies the proteostatic network of cancer cells. Expression analysis of HSF1 and other proteostatic components showed that p53 aggregation alone could account for >20% of the cancer-related heat shock response, in addition to hampering basal proteasomal degradation. Interestingly, increased HSF1 activation, which is also observed upon protein aggregation in neurodegeneration [54], plays a major role during oncogenesis, when cancer cells become 'addicted' to increased levels of chaperones, in part because of overactivation of HSF1 [48,55,56]. An increase in protein synthesis has been suggested to be a 'malignant' heat shock driver mechanism in cancer [57]. Our findings demonstrate that p53 aggregation also contributes significantly to this process, but also suggest that the aggregation of other, yet to be identified proteins may contribute to HSF1 dysregulation.

How does p53 aggregation affect the clinical outcome of patients? This needs to be addressed by large and carefully designed clinical studies. This first exploratory analysis suggests that grouping tumours into nIB-positive versus nIB-negative groups provided stratification with a worse outcome for patients bearing nIB-positive tumours, as opposed to a classification by genotype alone. Accordingly, patient biopsies containing nIBs also showed a shift in the proteostatic network, further demonstrating that nIBs highlight proteostatically altered, malignant tumour cells. Such tumours could possibly benefit the most from recently described therapeutics that clear mutant p53 from the cancer cell [19,58]. Other p53-targeted strategies [59] that aim at activating p53 could also benefit from these observations to identify eligible patients.

Overall, p53-nIBs should be considered as a hallmark of enhanced malignancy, which results from the interplay of p53 inactivation, mutation, accumulation, and aggregation, and tumour-associated stress. Beyond the large difference in disease aetiology, these findings also suggest unexpected parallels between cancer and neurodegeneration at the level of proteostatic regulation of cells, and strategies for the treatment of amyloid-associated diseases might therefore be equally beneficial for the treatment of cancer.

Acknowledgements

The Switch Laboratory was supported by grants from the Flanders Institute for Biotechnology (VIB), the University of Leuven (KU Leuven), the Research Foundation Flanders (FWO), the Flanders Agency for Innovation by Science and Technology (IWT), and the Federal Office for Scientific Affairs of Belgium (Belspo), IUAP P7/16. JS was supported by the European Research Council under the European Union's Horizon 2020 Framework Programme, ERC Grant agreement 647458 (MANGO). FDS is funded as a postdoctoral researcher by the FWO. EN and BH are funded by the IWT. MH was supported by the European Commission under Grant FP7 GA ERC-2012-SyG_318987–ToPAG. The SP8x confocal microscope is part of the InfraMouse core facility (KU Leuven-VIB) through a Hercules type 3 project (ZW09-03). The InCell Analyzer 2000 was made accessible by the Light Microscopy and Imaging Network (LiMoNe), which is part of the VIB Bio-Imaging core at KU Leuven. Next-generation sequencing and downstream mutation analysis were performed at the VIB Nucleomics Core. The authors thank Dr P. Nilsson and Dr P. Hammarstrom (Linköping, Sweden) for providing the luminescent conjugated oligothiophene (LCO) probes. The authors also thank all members of the Switch Laboratory and Professor F. Ulrich Hartl for helpful discussions. We thank Markus Oster and Martin Spitaler from the MPIB Imaging Facility for assistance with flow cytometry.

Author contributions statement

The authors contributed in the following way: FDS, TL, EN, BH: performed cellular and biochemical analyses;

FDS, MSR: performed all immunofluorescent tissue staining, scoring of patient samples, and sequencing and expression analysis; GDB: performed the computational analysis; DH, AD: performed surgeries and collected colon cancer patient data in Leuven, Belgium; XS: selected patient materials from the University Hospitals Leuven Pathology biobank, and performed the chromogenic p53 staining, analysis and scoring of DAB staining in colon cancer samples; MH: performed UbGFP analysis; JDB, LS: performed microarray analysis; SP: performed RNA sequencing analysis; SL, FA: provided the gynaecological tumour samples; KL, SR, LR, SC: collected biopsies and information of GBM patients; CS, PVDB, MW, MVE: provided colon cancer samples; FDS, JS, FR: designed the study, performed statistical analysis, and wrote the manuscript.

References

1. Hipp MS, Park SH, Hartl FU. Proteostasis impairment in protein-misfolding and -aggregation diseases. *Trends Cell Biol* 2014; **24:** 506–514.
2. Takalo M, Salminen A, Soininen H, *et al.* Protein aggregation and degradation mechanisms in neurodegenerative diseases. *Am J Neurodegener Dis* 2013; **2:** 1–14.
3. Eisele YS, Monteiro C, Fearns C, *et al.* Targeting protein aggregation for the treatment of degenerative diseases. *Nat Rev Drug Discov* 2015; **14:** 759–780.
4. Walther DM, Kasturi P, Zheng M, *et al.* Widespread proteome remodeling and aggregation in aging C. elegans. *Cell* 2015; **161:** 919–932.
5. Olivier M, Hollstein M, Hainaut P. TP53 mutations in human cancers: origins, consequences, and clinical use. *Cold Spring Harb Perspect Biol* 2010; **2:** a001008.
6. Bullock AN, Henckel J, Fersht AR. Quantitative analysis of residual folding and DNA binding in mutant p53 core domain: definition of mutant states for rescue in cancer therapy. *Oncogene* 2000; **19:** 1245–1256.
7. Muller PA, Vousden KH. Mutant p53 in cancer: new functions and therapeutic opportunities. *Cancer Cell* 2014; **25:** 304–317.
8. Robles AI, Harris CC. Clinical outcomes and correlates of TP53 mutations and cancer. *Cold Spring Harb Perspect Biol* 2010; **2:** a001016.
9. Zheng T, Wang J, Zhao Y, *et al.* Spliced MDM2 isoforms promote mutant p53 accumulation and gain-of-function in tumorigenesis. *Nat Commun* 2013; **4:** 2996.
10. Ano Bom AP, Rangel LP, Costa DC, *et al.* Mutant p53 aggregates into prion-like amyloid oligomers and fibrils: implications for cancer. *J Biol Chem* 2012; **287:** 28152–28162.
11. Forget KJ, Tremblay G, Roucou X. p53 Aggregates penetrate cells and induce the co-aggregation of intracellular p53. *PloS One* 2013; **8:** e69242.
12. Joerger AC, Fersht AR. Structural biology of the tumor suppressor p53. *Annu Rev Biochem* 2008; **77:** 557–582.
13. Lasagna-Reeves CA, Clos AL, Castillo-Carranza D, *et al.* Dual role of p53 amyloid formation in cancer; loss of function and gain of toxicity. *Biochem Biophys Res Commun* 2013; **430:** 963–968.
14. Levy CB, Stumbo AC, Ano Bom AP, *et al.* Co-localization of mutant p53 and amyloid-like protein aggregates in breast tumors. *Int J Biochem Cell Biol* 2011; **43:** 60–64.
15. Wang G, Fersht AR. First-order rate-determining aggregation mechanism of p53 and its implications. *Proc Natl Acad Sci USA* 2012; **109:** 13590–13595.
16. Wilcken R, Wang G, Boeckler FM, *et al.* Kinetic mechanism of p53 oncogenic mutant aggregation and its inhibition. *Proc Natl Acad Sci USA* 2012; **109:** 13584–13589.
17. Xu J, Reumers J, Couceiro JR, *et al.* Gain of function of mutant p53 by coaggregation with multiple tumor suppressors. *Nat Chem Biol* 2011; **7:** 285–295.
18. Yang-Hartwich Y, Soteras MG, Lin ZP, *et al.* p53 protein aggregation promotes platinum resistance in ovarian cancer. *Oncogene* 2015; **34:** 3605–3616.
19. Soragni A, Janzen DM, Johnson LM, *et al.* A designed inhibitor of p53 aggregation rescues p53 tumor suppression in ovarian carcinomas. *Cancer Cell* 2016; **29:** 90–103.
20. Nilsson KP, Ikenberg K, Aslund A, *et al.* Structural typing of systemic amyloidoses by luminescent-conjugated polymer spectroscopy. *Am J Pathol* 2010; **176:** 563–574.
21. De Genst E, Messer A, Dobson CM. Antibodies and protein misfolding: from structural research tools to therapeutic strategies. *Biochim Biophys Acta* **2014**; 1844**:** 1907–1919.
22. Abbas T, Dutta A. p21 in cancer: intricate networks and multiple activities. *Nat Rev Cancer* 2009; **9:** 400–414.
23. Degenhardt K, Chen G, Lindsten T, *et al.* BAX and BAK mediate p53-independent suppression of tumorigenesis. *Cancer Cell* 2002; **2:** 193–203.
24. Wu L, Levine AJ. Differential regulation of the p21/WAF-1 and mdm2 genes after high-dose UV irradiation: p53-dependent and p53-independent regulation of the mdm2 gene. *Mol Med* 1997; **3:** 441–451.
25. Brosh R, Rotter V. When mutants gain new powers: news from the mutant p53 field. *Nat Rev Cancer* 2009; **9:** 701–713.
26. Gannon JV, Greaves R, Iggo R, *et al.* Activating mutations in p53 produce a common conformational effect. A monoclonal antibody specific for the mutant form. *EMBO J* 1990; **9:** 1595–1602.
27. Breydo L, Uversky VN. Structural, morphological, and functional diversity of amyloid oligomers. *FEBS Lett* 2015; **589:** 2640–2648.
28. Yuan J, Xiao X, McGeehan J, *et al.* Insoluble aggregates and protease-resistant conformers of prion protein in uninfected human brains. *J Biol Chem* 2006; **281:** 34848–34858.
29. Polverino de Laureto P, Taddei N, Frare E, *et al.* Protein aggregation and amyloid fibril formation by an SH3 domain probed by limited proteolysis. *J Mol Biol* 2003; **334:** 129–141.
30. Mc Donald JM, Savva GM, Brayne C, *et al.* The presence of sodium dodecyl sulphate-stable Abeta dimers is strongly associated with Alzheimer-type dementia. *Brain* 2010; **133:** 1328–1341.
31. McDonald JM, Cairns NJ, Taylor-Reinwald L, *et al.* The levels of water-soluble and triton-soluble Abeta are increased in Alzheimer's disease brain. *Brain Res* 2012; **1450:** 138–147.
32. Lebedev I, Nemajerova A, Foda ZH, *et al.* A novel in vitro CypD-mediated p53 aggregation assay suggests a model for mitochondrial permeability transition by chaperone systems. *J Mol Biol* 2016; **428:** 4154–4167.
33. Lin JT, Chang WC, Chen HM, *et al.* Regulation of feedback between protein kinase A and the proteasome system worsens Huntington's disease. *Mol Cell Biol* 2013; **33:** 1073–1084.
34. Bersuker K, Hipp MS, Calamini B, *et al.* Heat shock response activation exacerbates inclusion body formation in a cellular model of Huntington disease. *J Biol Chem* 2013; **288:** 23633–23638.
35. Gies E, Wilde I, Winget JM, *et al.* Niclosamide prevents the formation of large ubiquitin-containing aggregates caused by proteasome inhibition. *PloS One* 2010; **5:** e14410.
36. Zimber A, Nguyen QD, Gespach C. Nuclear bodies and compartments: functional roles and cellular signalling in health and disease. *Cell Signal* 2004; **16:** 1085–1104.
37. Miki Y, Mori F, Kon T, *et al.* Accumulation of the sigma-1 receptor is common to neuronal nuclear inclusions in various neurodegenerative diseases. *Neuropathology* 2014; **34:** 148–158.

38. Bernardi R, Scaglioni PP, Bergmann S, *et al.* PML regulates p53 stability by sequestering Mdm2 to the nucleolus. *Nat Cell Biol* 2004; **6:** 665–672.
39. Haupt S, di Agostino S, Mizrahi I, *et al.* Promyelocytic leukemia protein is required for gain of function by mutant p53. *Cancer Res* 2009; **69:** 4818–4826.
40. Fogal V, Gostissa M, Sandy P, *et al.* Regulation of p53 activity in nuclear bodies by a specific PML isoform. *EMBO J* 2000; **19:** 6185–6195.
41. Guo A, Salomoni P, Luo J, *et al.* The function of PML in p53-dependent apoptosis. *Nat Cell Biol* 2000; **2:** 730–736.
42. Pearson M, Carbone R, Sebastiani C, *et al.* PML regulates p53 acetylation and premature senescence induced by oncogenic Ras. *Nature* 2000; **406:** 207–210.
43. Fu L, Gao YS, Tousson A, *et al.* Nuclear aggresomes form by fusion of PML-associated aggregates. *Mol Biol Cell* 2005; **16:** 4905–4917.
44. Mendillo ML, Santagata S, Koeva M, *et al.* HSF1 drives a transcriptional program distinct from heat shock to support highly malignant human cancers. *Cell* 2012; **150:** 549–562.
45. Hipp MS, Patel CN, Bersuker K, *et al.* Indirect inhibition of 26S proteasome activity in a cellular model of Huntington's disease. *J Cell Biol* 2012; **196:** 573–587.
46. Bence NF, Sampat RM, Kopito RR. Impairment of the ubiquitin–proteasome system by protein aggregation. *Science* 2001; **292:** 1552–1555.
47. Dantuma NP, Lindsten K, Glas R, *et al.* Short-lived green fluorescent proteins for quantifying ubiquitin/proteasome-dependent proteolysis in living cells. *Nat Biotechnol* 2000; **18:** 538–543.
48. Dai C, Whitesell L, Rogers AB, *et al.* Heat shock factor 1 is a powerful multifaceted modifier of carcinogenesis. *Cell* 2007; **130:** 1005–1018.
49. Lallemand-Breitenbach V, de The H. PML nuclear bodies. *Cold Spring Harb Perspect Biol* 2010; **2:** a000661.
50. Latonen L, Moore HM, Bai B, *et al.* Proteasome inhibitors induce nucleolar aggregation of proteasome target proteins and polyadenylated RNA by altering ubiquitin availability. *Oncogene* 2011; **30:** 790–805.
51. Lee HJ, Gutierrez-Garcia R, Vilchez D. Embryonic stem cells: a novel paradigm to study proteostasis? *FEBS J* 2017; **284:** 391–398.
52. Audas TE, Audas DE, Jacob MD, *et al.* Adaptation to stressors by systemic protein amyloidogenesis. *Dev Cell* 2016; **39:** 155–168.
53. Onozuka H, Tsuchihara K, Esumi H. Hypoglycemic/hypoxic condition in vitro mimicking the tumor microenvironment markedly reduced the efficacy of anticancer drugs. *Cancer Sci* 2011; **102:** 975–982.
54. Neef DW, Jaeger AM, Thiele DJ. Heat shock transcription factor 1 as a therapeutic target in neurodegenerative diseases. *Nat Rev Drug Discov* 2011; **10:** 930–944.
55. Whitesell L, Lindquist S. Inhibiting the transcription factor HSF1 as an anticancer strategy. *Expert Opin Ther Targets* 2009; **13:** 469–478.
56. Santagata S, Xu YM, Wijeratne EM, *et al.* Using the heat-shock response to discover anticancer compounds that target protein homeostasis. *ACS Chem Biol* 2012; **7:** 340–349.
57. Santagata S, Mendillo ML, Tang YC, *et al.* Tight coordination of protein translation and HSF1 activation supports the anabolic malignant state. *Science* 2013; **341:** 1238303.
58. Alexandrova EM, Yallowitz AR, Li D, *et al.* Improving survival by exploiting tumour dependence on stabilized mutant p53 for treatment. *Nature* 2015; **523:** 352–356.
59. Verreault M, Schmitt C, Goldwirt L, *et al.* Preclinical efficacy of the MDM2 inhibitor RG7112 in MDM2-amplified and TP53 wild-type glioblastomas. *Clin Cancer Res* 2016; **22:** 1185–1196.
*60. Schymkowitz J, Borg J, Stricher F, *et al.* The FoldX web server: an online force field. *Nucleic Acids Res* 2005; **33:** W382–W388.
*61. Wagle N, Berger MF, Davis MJ, *et al.* High-throughput detection of actionable genomic alterations in clinical tumor samples by targeted, massively parallel sequencing. *Cancer Discov* 2012; **2:** 82–93.
*62. Geiss GK, Bumgarner RE, Birditt B, *et al.* Direct multiplexed measurement of gene expression with color-coded probe pairs. *Nat Biotechnol* 2008; **26:** 317–325.
*63. Hipp MS, Bersuker K, Kopito RR. Live-cell imaging of ubiquitin–proteasome system function. *Methods Mol Biol* 2012; **832:** 463–472.
*64. Park SH, Kukushkin Y, Gupta R, *et al.* PolyQ proteins interfere with nuclear degradation of cytosolic proteins by sequestering the Sis1p chaperone. *Cell* 2013; **154:** 134–145.
*65. Maurer-Stroh S, Debulpaep M, Kuemmerer N, *et al.* Exploring the sequence determinants of amyloid structure using position-specific scoring matrices. *Nat Methods* 2010; **7:** 237–242.

*Cited only in supplementary material.

SUPPLEMENTARY MATERIAL ONLINE

Supplementary materials and methods

Figure S1. Expression analysis of p53 in tumour tissue sections

Figure S2. Expression analysis of the aggregation marker A11, p21 and BAX

Figure S3. Biochemical analysis of the p53 protein

Figure S4. Functional and cellular analysis of the p53 protein in endogenous tumour cell lines

Figure S5. Aggregated p53 alters the proteostatic network of cancer cells

Figure S6. Genetic and western blot analysis of p53 knockout tumour cells

Figure S7. Survival analysis of clinical cohort of colon cancer patients and expression analysis

Table S1. Correlation between the p53 inclusion status in the primary colon tumour and metastatic tumour cells in the lymph nodes

Table S2. Genotype analysis of 92 patients

Table S3. Cross-section of p53 genotype and p53 immunofluorescence analysis in colon cancer and glioblastoma

Table S4. List of the significantly correlated proteostatic genes from a pan-cancer microarray analysis

Table S5. Clinical parameters of the cohort of colon cancer patients

Table S6. Clinical parameters of the cohort of glioblastoma patients